A shallow layer model for heavy gas dispersion from natural sources: application and hazard assessment at Caldara di Manziana, Italy.

A. Costa[1], G. Chiodini[1], D. Granieri[1], A. Folch[1], R.K.S. Hankin[2], S. Caliro[1], R. Avino[1], C. Cardellini[3]

[1] Osservatorio Vesuviano-INGV, Napoli, Italy.

[2] National Oceanography Centre, Southampton, UK.

[3] Dipartimento Scienze della Terra, Università di Perugia, Italy.

Abstract

Several non-volcanic sources in central Italy emit a large amount of carbon dioxide (CO_2). Under stable atmospheric conditions and/or in presence of topographic depressions, the concentration of CO_2, which has a molecular mass greater than that of air, can reach high values that are lethal to humans or animals. Several episodes of this phenomenon were recorded in central Italy and elsewhere. In order to validate a model for the dispersion of a heavy gas and to assess the consequent hazard, we applied and tested the code TWODEE-2, an improved version of the established TWODEE model, which is based on a shallow layer approach that uses depth-averaged variables to describe the flow behavior of dense gas over complex topography. We present results for a vented CO_2 release at Caldara di Manziana in central Italy. We find that the model gives reliable results when the input quantity can be properly defined. Moreover, we show that the model can be a useful tool for gas hazard assessment, by evaluating where and when lethal concentrations for humans and animal are reached.

1 Introduction

Recent studies have shown that the Western regions of central and South Italy are affected by an intense CO_2 degassing process. The origin of this CO_2 is still a debated matter. From petrologic and petrographic investigations, Gianelli (1985) proposed a metamorphic origin for the CO_2 released in Tuscany by high temperature geothermal systems (*i.e.*, Larderello and Amiata). More recently, Chiodini et al. (2004) showed that the CO_2 anomaly affects almost continuously the central and the southern part of Italy, from the Tyrrhenian coast to the Apennine belt (Fig. 1). They inferred the presence of a very large flux of deeply derived CO_2 (~ 25,000 t d^{-1} equivalent to ~ 10% of the estimated CO_2 globally emitted from sub-aerial volcanoes). A shallow crustal metamorphic source for all regional CO_2 Earth degassing seemed to be inappropriate for these authors and they proposed a mantle-derived origin of the CO_2 linked to the presence of a mantle metasomatised by crustal fluids originating from a down-going slab containing crustal derived carbon (e.g., limestone, calcareous flysch formations) (Chiodini et al., 2000; 2004, Collettini et al., 2007).

More than one hundred cold CO_2-rich gas emissions are formed at the surface as a consequence of this deep process (e.g., Chiodini et al. 2000, 2004, Minissale 2004, Rogie et al. 2000). Many of these emissions have very high gas flow rates. For example, areas such as Mefite d'Ansanto, Poggio d'Olivo or Caldara di Manziana in Central-South Italy, have gas flow rates of the order of hundreds t d^{-1} (Rogie et al. 2000), similar to diffuse degassing from active volcanoes in quiescence stage (i.e., Vulcano, Granieri et al., 2006; Nisyros, Caliro et al., 2005; Vesuvio, Frondini et al., 2004; Solfatara, Chiodini et al., 2001).

The main constituent of all gas emissions is carbon dioxide which is denser than air at the relatively cold discharge temperatures. During certain meteorological conditions (low wind speeds, high atmospheric pressures, etc.) the gas tends to accumulate in morphological depressions thus forming invisible and lethal traps. At high concentrations carbon dioxide is, in fact, toxic and dangerous to humans and animals (see Table 1). One of the most tragic events of

gas release occurred at Lake Nyos (Cameroon) on 21 August 1986, when a dense cloud of carbon dioxide hugging the ground suffocated more than 1700 people and an uncounted number of animals in just one night (Giggenbach, 1990; Giggenbach et al., 1991; Clarke, 2001). A previous case (1984) was the sudden CO_2 release from Monoun Lake (~ 100 km to the SSE of Lake Nyos), that killed 37 people (Giggenbach et al., 1991; Sigurdsson et al., 1987). A similar tragic event was the lethal gas (largely CO_2) burst from Dieng Volcanic Complex (Indonesia) in February 1979 when 149 people were killed by a cloud of gas (Giggenbach et al., 1991; LeGuern et al., 1979). In the area of Mammoth Mountain (CA, USA) anomalous CO_2 discharge from soils occurred in 1990 (Gerlach et al., 1998; Rogie et al., 1998), killing trees in several areas (about 50 ha), and posing a health hazard to the resort site. Near asphyxia incidents involving people staying in confined spaces between 1990 and 1994 were ascribed to CO_2 soil degassing (Baxter et al., 1999).

Several similar episodes were recorded also in Italy (Rogie et al., 2000). At Mefite d'Ansanto (Campania) three people were killed during the 1990's and historical chronicles describe the death of many others during the 17th century. The gas emitted by the CO_2 saturated water of Tivoli springs, located near Rome, killed several boys during the 1970's. At Colli Albani (Rome), many lethal accidents have involved animals and people. The most recent accidents caused the death by asphyxia of 29 cows on September 1999, five sheep on March 2000 and a man on December 2000 (Carapezza et al., 2003). At Veiano (Latium) the gas killed two hunters in 1991. The most recent recorded lethal accident occurred at Mt Amiata (Siena) in November 2003 when a hunter was killed by the CO_2 discharged by one of the many emissions of the area. This list is impressive considering that it is largely incomplete because a specific research on the accidents caused by the gas has never been done. It is worth noting that in the case of Italian emissions the gas toxicity is increased by a variable amount of H_2S concentrations which in some cases can be as high as a few percent. Hydrogen sulfide in fact can have sudden lethal effects at relatively low concentration, such as 700 ppm (Beaubien et al., 2003).

In the frame of gas hazard mitigation in Italy, the specific aim of this research is to investigate the CO_2 dispersion into the atmosphere under different topographic and meteorological conditions, developing and validating a tool for gas dispersion forecasting and hazard assessment.

In this study we used a FORTRAN 90 code (Folch et al., 2007), named TWODEE-2, which has been derived from the improvement and optimization of the original shallow layer model TWODEE developed by Hankin and Britter (1999a, 1999b, 1999c). TWODEE has been applied to risk assessment of industrially realistic problems for both continuous (Hankin 2004a) and instantaneous (Hankin, 2004b) releases over complex topography; the model is able to simulate heavy gas flow in a calm ambient and has been validated against experiments (Hankin 2003b, 2003c).

The paper is organized in two main sections. First we describe the heavy gas transport model adopted. Then we discuss the results obtained by the application of the model to a real case. For this purpose the area of Caldara di Manziana (CdM, Italy), one of the biggest manifestation of Central Italy, was selected (Fig. 2). The CO_2 soil source fluxes were evaluated during a field campaign performed in June 2006. An automatic station was operative at CdM from 5 to 6 February 2007 in order to collect meteorological data and CO_2 concentration on air (see table in electronic appendix). These parameters are needed by the gas dispersion model. Finally, we discuss some implications of the model application and its potential use for hazard assessment.

2 Shallow Layer Dense Gas Transport Model

The cloud dispersion of gas denser than air released from a given source is governed by gravity and by lateral eddies, the latter increase the mixing with surrounding air at the edges of the cloud, decreasing its density. During the initial dispersion phase, negative buoyancy controls the gas movement and the cloud simply follows the ground (gravitational phase). In contrast, when the density contrast becomes less important, gas dynamics is basically controlled by the

wind and the atmospheric turbulence (passive dispersion phase). In the last case, simulations can be carried out using simplified approaches (e.g., Costa et al., 2005).

In theory, gas dispersion can be studied by solving the transport equations for mass, momentum and energy. However, in practice, because the demanding computational requests, different simplified models that only partially describe the physics are commonly used. These models range from simpler analytical or similarity approaches to more complex Computational Fluid Dynamics (CFD) models. A common approach is given by the Box (or Similarity) models (Hankin, 2003a) which describe the integral properties of a plume. A set of differential equations for averaged mass, momentum and energy balance is solved along the plume using different simplifying similarity assumptions (e.g., Blackmore et al., 1982). DEGADIS (Spicer and Havens, 1989), SLAB (Ermak, 1990) and HEGADAS (Witlox, 1994) are popular examples of these kind of models. The most complete but computationally most expensive models are the three-dimensional CFD models based on the transport theory of mass, momentum, energy and species (e.g., Costa and Macedonio, 2002). This approach is able to simulate dispersion of heavy gases accounting for obstacles and topographic effects, variation of atmospheric conditions and wind direction. Unfortunatelly its computational requirements constrain its use in many practical cases.

A compromise between the complexity of CFD models and the simpler integral models is given by the shallow layer approach which uses depth-averaged variables to describe the flow behavior (Hankin and Britter, 1999a, 1999b, 1999c; Venetsanos et al., 2003). As we will show, these models are able to describe gravity driven flows of dense gas over a complex topography.

At present, applications of Shallow Water Equations (SWE) cover a wide range of problems which have important implications for hazard assessment, from flood simulation (*e.g.*, Burguete et al., 2002) to propagation of tsunamis (Heinrich et al., 2001). SWE are valid in the limit $H_*^2/L_*^2 << 1$, where H_* is the undisturbed fluid height and L_* is the characteristic wave length scale in the flow direction. This means that we are dealing with very long waves.

The TWODEE-2 model is based on depth-averaged equations obtained by integrating mass, density and momentum balance equations over the fluid depth, from the bottom up to the free surface. This approach is able to describe the cloud as a function of time and of the two-dimensional ground positions in terms of four variables: cloud depth, two depth-averaged horizontal velocities, and depth-averaged cloud concentration. Thermodynamic effects such as condensation are not included at present but further development could account for them by introducing an additional equation for gas enthalpy.

2.1 Depth averaged variables

Differently from fluids commonly described by SWE, real gas clouds do not have a definite upper surface. As a consequence, it is necessary to define the cloud depth, *h*, in terms of the vertical concentration distribution $\rho(z)$. In fact, we must point out that the actual vertical concentration profile is not uniform as for fluids, but it is characterized by an exponential decay (Hankin and Britter, 1999a, 1999b, 1999c). Depth averaged values of gas density $\overline{\rho}$ and velocities $(\overline{u};\overline{v})$ must therefore be defined in terms of their vertical distributions $\rho(z)$ and $(u(z);v(z))$.

We consider the cloud depth as that height below which some fraction α of the buoyancy $g(\rho-\rho_a)$ is located:

$$\int_{z=0}^{h} g(\rho(z)-\rho_a)dz \equiv \alpha \int_{z=0}^{\infty} g(\rho(z)-\rho_a)dz \qquad (1)$$

where a α value of 0.95 has been adopted (Hankin and Britter, 1999a), *g* stands for gravity acceleration and ρ_a is the air density. Concerning the depth-averaged density we have:

$$h(\overline{\rho}-\rho_a) \equiv \int_{z=0}^{\infty} (\rho(z)-\rho_a)dz \qquad (2)$$

In similar way, the depth-averaged velocities $(\overline{u},\overline{v})$ are given by the relationships:

$$h(\overline{\rho}-\rho_a)\overline{u} \equiv \int_{z=0}^{\infty}(\rho(z)-\rho_a)u(z)dz \tag{3}$$

$$h(\overline{\rho}-\rho_a)\overline{v} \equiv \int_{z=0}^{\infty}(\rho(z)-\rho_a)v(z)dz \tag{4}$$

Concerning the vertical concentration profile, Hankin and Britter (1999b) showed how it can be calculated in terms of the depth average density $\overline{\rho}$ and an empirical parameter S_1 as:

$$\rho(z)-\rho_a = (\overline{\rho}-\rho_a)\frac{2}{S_1}\exp\left(-\frac{2}{S_1}\frac{z}{h}\right) \tag{5}$$

From (5) we can directly evaluate the gas concentration c as:

$$c(z) = c_b + (10^6 - c_b)\times\frac{\rho(z)-\rho_a}{\rho_g-\rho_a} \tag{6}$$

where c is expressed in parts per million (ppm) and c_b is the background concentration (see Folch et al., 2007 for further details).

2.2 Depth Averaged Equations

Assuming an incompressible homogeneous fluid and a hydrostatic pressure distribution, the SWE for a uniform or gradually varied flow are given by (*e.g.*, Hankin and Britter, 1999):

$$\frac{\partial h}{\partial t}+\frac{\partial h\overline{u}}{\partial x}+\frac{\partial h\overline{v}}{\partial y} = u_{entr} \tag{7}$$

$$\frac{\partial h(\overline{\rho}-\rho_a)}{\partial t}+\frac{\partial h(\overline{\rho}-\rho_a)\overline{u}}{\partial x}+\frac{\partial h(\overline{\rho}-\rho_a)\overline{v}}{\partial y} = \rho_a u_{entr} \tag{8}$$

$$\begin{aligned}&\frac{\partial h\overline{\rho u}}{\partial t}+\frac{\partial h\overline{\rho}\overline{u}^2}{\partial x}+\frac{\partial h\overline{\rho}\overline{u}\overline{v}}{\partial y}+\frac{1}{2}S_1\frac{\partial g(\overline{\rho}-\rho_a)h^2}{\partial x}+S_1 g(\overline{\rho}-\rho_a)h\frac{\partial e}{\partial x}+\\ &\frac{1}{2}\rho C_D\overline{u}|\overline{\mathbf{u}}|+V_x+k\rho_a\left(\frac{\partial}{\partial t}+u_a\frac{\partial}{\partial x}+v_a\frac{\partial}{\partial y}\right)[h(\overline{u}-u_a)] = u_{entr}\rho_a u_a\end{aligned} \tag{9}$$

$$\frac{\partial h\overline{\rho v}}{\partial t}+\frac{\partial h\overline{\rho}\overline{v}^2}{\partial y}+\frac{\partial h\overline{\rho}\overline{u}\overline{v}}{\partial x}+\frac{1}{2}S_1\frac{\partial g(\overline{\rho}-\rho_a)h^2}{\partial y}+S_1 g(\overline{\rho}-\rho_a)h\frac{\partial e}{\partial y}+$$
$$\frac{1}{2}\rho C_D\overline{v}|\overline{\mathbf{u}}|+V_y+k\rho_a\left(\frac{\partial}{\partial t}+u_a\frac{\partial}{\partial x}+v_a\frac{\partial}{\partial y}\right)[h(\overline{v}-v_a)]=u_{entr}\rho_a v_a \qquad (10)$$

Here t denotes time, x and y the horizontal coordinates u_{entr} the entrainment rate of air, $e=e(x,y)$ is the terrain elevation, S_1 is a shape factor, C_D is a skin friction coefficient, $(V_x;V_y)$ indicates the turbulent shear stress exerted on the cluoud, and k is a semi-empirical parameter. Eq. (7) represents volume conservation of dense fluid, eq. (8) represents the mass conservation for the general case of a variable gas density and, finally, eqs. (9) and (10) represent the momentum balance for the gas clouds. TWODEE-2 is based on the numerical solution of the governing equations (7) to (10). The numerical method is based on the Flux Corrected Transport (FCT) scheme of Zalesak (1979). This scheme combines the low numerical diffusion of high order schemes with the absence of numerical oscillations typical of low order schemes. Fundamentally, FCT calculates the fluxes between adjacent elements using a weighted average of flux as computed by a low order scheme and a high order scheme. The weighting is done in such a manner as to use the high order scheme unless doing so would result in the creation of overshoots (that is, new extrema in the advected quantity) not predicted by the low order scheme. The assumption is therefore that any new extrema predicted by the low order scheme are genuine. In this paper we assume that the wind is horizontally uniform and described by the classical similarity theory along the vertical direction. Thus the wind velocity profile is expressed in terms of the roughness length z_0, the friction velocity u_*, and the Monin-Obukhov length L:

$$U_a(z)=\frac{u_*}{K}\left[\ln\left(\frac{z}{z_0}\right)-\psi_m\left(\frac{z}{L}\right)\right] \qquad (11)$$

where K is the von Karman constant ($K=0.4$) and ψ_m is the classical stability function for momentum (e.g., Jacobson, 1999). For a more detailed description of the equations see Hankin

and Britter (1999); for the numerical parameters and further details about the code see Folch et al. (2007).

The assumption of a uniform wind field is appropriate for our experiment because the distance between the meteorological station and the main sources is short and the topography is mainly flat (see Fig. 2). However, when the computational domain is large and the terrain domain is complex and large, the uniform wind assumption is no longer valid. In that case, there is the option in TWODEE-2 for coupling the gas dispersion model with a zero-divergence wind field that incorporates local terrain effects, such as the wind fields furnished by a mass consistent meteorological processors (see Folch et al., 2007).

3 Model Applications

In this section we show two applications of the model described above. The first consists of an application/validation of the model for a case when we have a very refined definition of source, topography and wind. In the second case, we show an application of TWODEE-2 for hazard assessment purposes.

3.1 Test Site: Caldara di Manziana, Italy

Caldara di Manziana (CdM) is a sub-circular structure of ~ 0.25 km^2 located ~ 20 km NW of Rome (Fig. 2), genetically related to the alkali-potassic volcanism which affected central Italy since 0.6 Ma. The origin of this structure is still debated but Rogie et al. (2000) hypothesized that CdM is a crater formed by a hydrothermal explosion. The floor of the crater is almost flat and broad and it is elongated (~500 m fetch) and open towards SW. The gently sloping rim of the crater is elevated few tens of meters. CdM, declared Natural Monument by the Italian Authorities on 1988, is regularly frequented by people and visited by several wild species (wild boars, foxes, hedgehogs), mainly during nighttime hours. At present there is intense degassing of CO_2 in this area. The emission occurs both as focused vents from water pools, the main of which sustains a

0.5 m high water column ('CO_2 vent' in Fig. 2 and video in the electronic appendix), as well as soil diffuse degassing from the crater floor. No human accidents caused by gas toxicity have been reported, but dead wild animals have been found several times.

To test the computational model we performed an experiment at CdM in an area close to the water pool which represents the main point source of CO_2 inside the crater (Fig. 2).

3.2 Input Data: Topography and Gas Flux

The simulation of gas dispersion using the TWODEE-2 code requires the topography grid, gas fluxes and wind data as input parameters (Folch et al., 2007). The topography of the area was defined by assigning at each cell the correspondent topographic height derived from the 1:25000 topography map. The location and the flux of the gas sources on the computational domain have been defined by means of a specific CO_2 flux survey. The survey was performed from 12 to 14 June 2006 when 538 CO_2 flux measurements were obtained using an accumulation chamber. This measurement method allows a quick direct measurement of the CO_2 flux from soil (Chiodini et al., 1996, 1998; Evans et al., 2001; Welles et al., 2001). The measured soil flux values range from 2.3×10^{-8} kg m^{-2} s^{-1} to 2.8×10^{-4} kg m^{-2} s^{-1} with an average value of 7.7×10^{-6} kg m^{-2} s^{-1} (Fig 3). Based on the measurements, the fluxes of 11312 cells of size 8 m × 8 m, were simulated by the sGs algorithm (sequential Gaussian simulations, Deutsch and Journell, 1998) following the method described in Cardellini et al. (2003). The ensemble average of the total CO_2 output from 100 sGs simulations results in 1.88 ± 0.12 kg s^{-1}, a value very similar to the result of the previous July 1996 measurement campaign (1.85 kg s^{-1}; Chiodini et al., 1999; Rogie et al., 2000). In order to quantify all gas flux contribution, beside the diffuse degassing area (see Fig. 3) we estimated gas fluxes from both the main focused gas vent (CO_2 vent in Fig. 2), consisting in ~ 0.15 kg s^{-1} CO_2 (Rogie et al., 2000) and the contribution of a water pool located nearby to the main vent which we measured emitting ~ 0.023 kg s^{-1} CO_2. Therefore a total CO_2 output of ~ 2.03 kg s^{-1}

was estimated as contribution of both soil diffuse degassing from the floor of the crater, and from the two main punctual sources. Figure 3 shows the map of the soil CO_2 flux, resulting by the sGs simulations. The anomalous area is restricted to the central and northern portion of the CdM crater floor in the neighborhood of the main water pools affected by intense CO_2 degassing (white dots in the map).

3.3 Meteorological Measurements and Experiment Design

During the experiment carried out on 5 and 6 February 2007 we installed two automatic stations to measure, respectively, meteorological data and CO_2 concentration on air. Both stations were mounted on a tripod tower (Fig. 4) which was placed several tens of meters away from the highest degassing sources of the CdM (CO_2 vent in Fig. 2). Meteorological station acquired the barometric pressure, the air temperature and the wind speed (Fig. 4) for more than 15 hours, from 17:30 (local time, LT) of 5 February 2007 to 08:40 (LT) of 6 February 2007. Air temperature measurements were taken 0.30 and 2.90 m above the ground by a couple of antiradiant thermo-hygrometers at natural ventilation (DMA570, LSI S.p.A., Milano, Italy), which are able to measure also the air humidity. The resolution of the temperature sensors is 0.04°C. A laboratory inter-calibration of the two sensors was performed a week before the experiment. Atmospheric pressure was measured by a barometer (DQA240, LSI S.p.A., Milano, Italy) at 2.2 m above the soil. The wind sensor was a cup anemometer (DNA022, LSI S.p.A., Milano, Italy) which includes, in a single apparatus, both the transducers for measuring wind speed (range 0-60 ms^{-1}, resolution 0.05 ms^{-1} and accuracy 0.1 ms^{-1}) and wind direction (range 0-359°). Anemometer was located at 3.45 m above the ground. Meteorological data were acquired at a time interval of 10 seconds and averaged over a period of 10 minutes. During the same time span an open path infrared CO_2/H_2O analyzer (LI-7500, LI-COR Inc. Lincoln, Nebraska), mounted over the tower at 2.20 m above the ground, measured CO_2 concentration in air. The measurement accuracy is

1% of reading in the typical range of the factory calibration (0-3000 ppm) and lower for higher concentrations. The gas analyzer was calibrated prior to fieldwork (zero and span). Data were logged at 10-Hz rate and the average value was calculated over 10-min periods. Friction velocity u_* and Monin-Obukhov length L, appearing in eq. (11), were calculated using the non-iterative method of Louis (1979) which is based on the estimation of the bulk Richardson number (Jacobson, 1999):

$$Ri_b \approx \frac{g\left[\theta(z_{ref}) - \theta(z_0)\right](z_{ref} - z_0)}{\theta(z_0)\left[u_a^2(z_{ref}) + v_a^2(z_{ref})\right]} \qquad (12)$$

where $\theta = T\left(10^5\,\mathrm{Pa}/p\right)^{0.286}$ denotes the potential temperature (p in Pa). In our case we have a reference height $z_{ref} = 3.45\,\mathrm{m}$ and, since most of the soil in the area between the water pools and the station was mainly bare or covered of water (see inset in Fig. 2), we set a roughness height $z_0 = 0.005\,\mathrm{m}$.

3.4 Comparison between measured and computed concentrations

Using the input data described above, we applied the model to simulate the temporal evolution of the gas cloud during the same time interval as the measurements, *i.e.*, from 17:30 (LT) of 5 February 2007 to 08:40 (LT) of 6 February 2007. In this way we were able to compare directly the concentrations detected at the station (at 2.2 m height, every 10 minutes) with the simulation results at the same position. The calculated values are averages of a 25 m by 25 m squares. Fig. 5 shows the time evolution of both measured and computed concentrations which are in good agreement. Over the time span considered we observed the effects of the daytime-nighttime transition associated with an increase in gas concentration as the wind intensity decreases and an inversion in temperature. A view from above of the gas plume at 2.2 m height, showing the temporal evolution at different time slices is plotted on Fig. 6. Each frame of Fig. 6 also records

the corresponding wind velocity components, meteorological parameters and time after the modeling start (2h, 6h, 10h and 14h corresponding to a LT of 19:30, 23:30, 03:30 and 07:30 respectively). The 2h, 6h and 10h results represent the gas plume at low wind conditions (nocturnal conditions) while the last image (14h) is representative of relatively high wind values when the gas plume practically disappears during the morning. The first three images show that the shape of CO_2 plume during night (*i.e.*, at low wind conditions) is mainly controlled by topography. The plume follows the topography and is elongated towards SW, with a maximum width at the centre of the domain, where the floor of the CdM crater is broader. At the lowest wind values (6h) the plume slowly turns towards the SW part of the domain and is constricted by the topography into a narrow channel.

3.5 Hazard assessment and the most dangerous scenarios

The results obtained in the previous section indicate that the model is a reliable tool for forecasting gas dispersion. As a second application we use the model to establish whether the CO_2 concentration at CdM can reach values that are lethal for humans or animals (Table 1). In order to assess gas hazards we performed simulations assuming stable and very low wind conditions ($U_a < 0.1$ m/s, $z_{ref} / L > 10^3$) for a duration of ten hours at night. The resulting concentration maps the heights of 0.1 m and 1.50m are plotted in Fig. 7. These two heights were considered the possible levels of inhalation for small-size animals and humans, respectively. The model predicts that under this condition, the CO_2 concentration at 0.1 m height reaches maximum values of about 7% in an area near to the vent. These values indicate that concentrations of the order of 10% can be reached near the soil defining a potentially lethal region for small-size animals for exposures longer than 10-15 minutes (see Table 1). Moreover considering that at CdM H_2S constitutes ~ 1.2% of the gas emission and assuming the gas plume maintains a CO_2/H_2S ratio close to the original value, a concentration of about 5.5% of CO_2 would imply a

near lethal H_2S concentration of 700 ppm (Beaubien et al., 2003).

At 1.5 m height the model finds a maximum CO_2 concentration of about 3%, a value below the 5.5% threshold defined on the basis of the H_2S concentration and well below the pure CO_2 dangerous threshold for humans of 15% (Table 1). These results generally agree with the fact that at CdM accidents to humans were never recorded whereas some times small size animals killed by the gas were found.

Lethal conditions for humans at CdM requires a strong increase of CO_2 flux. For example, an increase of the soil CO_2 flux with as factor of five would cause, under the same meteorological conditions, large parts of CdM to achieve lethal CO_2 concentration at 1.5 m height (Table 1, Fig. 8). These results illustrate the capability of the model to investigate dangerous conditions for humans. However, the large increase of CO_2 flux necessary to reach these dangerous conditions is considered to be very improbable (although not impossible if, for example, the area would be affected by important seismic activity or by a volcanic unrest).

Model applications similar to those described above can be helpful in studying CO_2 concentration distribution under a variety of seepage scenarios and atmospheric conditions, as well as for predicting environmental risks from potential leakage and seepage related with accumulation of large quantities of injected CO_2 in geologic sequestration sites (*e.g.*, Oldenburg and Unger, 2003; 2004).

4 Conclusion

CO_2 emissions can be serious hazard in many areas of the world where natural degassing occurs as permanent manifestations or as episodic phenomena. Although the gas source can be reasonably well specified, the subsequent gas dispersion is a complex physical process affected by local topography, meteorology, surface roughness and atmospheric stability. We applied and tested the shallow layer model TWODEE-2 to simulate CO_2 dispersion over the Caldara di

Manziana, one of the many permanent gas emissions of Italy. We found that the modeling results reproduced measured concentrations well over a range of meteorological conditions. The reported applications show the potential of the TWODEE-2 model in assessing as the gas dispersion pattern affected by the terrain elevation, the ambient wind-speed and gas source variation.

References

Baxter, P. J., 2000. Gases. In: P. J. Baxter, P.H. Adams, T.-C. Aw, A. Cockcroft and J.M. Harrington (Editors), Hunter's Diseases of Occupations. Arnold, London, 123-178.

Baxter, P. J., Baubron, J-C., Coutinho, R., 1999. Health hazards and disaster potential of ground gas emissions at Furnas volcano, São Miguel, Azores. J. Volcanol. Geotherm. Res., 92 (1-2), 95-106.

Beaubien, S.E., Ciotoli, G., Lombardi, S., 2003. Carbon dioxide and radon gas hazard in the Alban Hills area (central Italy). J. Volcanol. Geotherm. Res., 123, 63-80.

Blackmore, D., Herman, M., Woodward, J., 1982. Heavy gas dispersion models. J. Hazard. Mater. 6, 107–128.

Burguete, J., Garcia-Navarro, P., Aliod, R., 2002. Numerical simulation of runoff from extreme rainfall events in a mountain water catchment. Nat. Haz. Earth Syst. Sci. 2, 109–117.

Carapezza, M. L., Badalamenti, B, Cavarra, L. and Scalzo, A. (2003). Gas hazard assessment in a densely inhabited area of Colli Albani volcano (Cava dei Selci, Roma). J. Volcanol. Geotherm. Res., 123 (1-2), 81-94.

Cardellini, C., Chiodini, G. and Frondini, F., 2003. Application of stochastic simulation to CO2 flux from soil: Mapping and quantification of gas release. J. Geophys. Res., 108(B9): 2425-2437.

Chiodini, G., Cardellini, C., Amato, A., Boschi, E., Caliro, S., Frondini, F. & Ventura, G. 2004. Carbon dioxide Earth degassing and seismogenesis in central and southern Italy. Geophys. Res. Lett., 31, L07615, doi:10.1029/2004GL019480.

Chiodini, G., Cioni, R., Guidi, M., Raco, B. and Marini, L., 1998. Soil CO2 flux measurements in volcanic and geothermal areas. Applied Geochemistry, 13(5): 543-552.

Chiodini, G., Frondini, F., Cardellini, C., Parello, F. & Peruzzi, L. 2000. Rate of diffuse carbon dioxide Earth degassing estimated from carbon balance of regional aquifers: The case of central Apennine, Italy. J. Geophys. Res.-Solid Earth, 105, 8423-8434.

Chiodini G., Frondini F., Cardellini C., Granieri D., Marini L., Ventura G. 2001. CO_2 Degassing and Energy Release at Solfatara Volcano, Campi Flegrei, Italy. J. Geophys. Res., 106 (B8): 16213-16221.

Chiodini, G., Frondini, F., Kerrick, D. M., Rogie, J., Parello, F., Peruzzi, L. & Zanzari, A. R. 1999. Quantification of deep CO_2 fluxes from Central Italy. Examples of carbon balance for regional aquifers and of soil diffuse degassing. Chemical Geology, 159, 205-222.

Chiodini, G., Frondini, F., Raco, B., 1996. Diffuse emission of CO2 from the Fossa crater, Vulcano Island (Italy). Bulletin of Volcanology, 58(1): 41-50.

Clarke, T., 2001. Taming Africa's killer lake. Nature 409, 554–555.

Collettini, C., Cardellini, C., Chiodini, G., De Paola, N., Holdsworth, R.E., Smith, S.A.F, 2007. Fault weakening due to CO2 involvement in the extension of the Northern Apennines: short- and long-term processes. The internal structures of fault zones: fluid flow and mechanical properties. Geological Society of London, Special Publication, in press.

Deutsch, C.V. and Journel, A.G., 1998. GSLIB: Geostatistical Software Library and Users Guide. Applied Geostatistics Series. Oxford Univerity Press, New York Oxford, 369 pp.

Douglas, S. and Kessler, R.C., 1990. User's Manual for the Diagnostic Wind Model, EPA-450/4-90-007C, ed. Carr, L., Volume III, San Rafael, CA, USA.

Ermak, D., 1990. User's manuals for SLAB: An atmospheric dispersion model for denser-then-air releases. Tech. rep., UCRL-MA-105607, Lawrence Livermore National Laboratory, CA.

Evans, W. C., M. L. Sorey, B. M. Kennedy, D. A. Stonestrom, J. D. Rogie, and D. L. Shuster.

2001 High CO_2 emissions through porous media: Transport mechanisms and implications for flux measurement and fractionation, Chem. Geol., 177(1– 2), 15–29.

Faivre-Pierret, R. and Le Guern, F., 1983. Health risks linked with inhalation of volcanic gases and aerosols. In: H. Tazieff and J.C. Sabroux (Editors), Forecasting Volcanic Events. Elsevier Science Publishers B.V., Amsterdam, 69-81.

Folch, A., Costa, A., Hankin, R.K.S.. 2007. TWODEE-2: a shallow layer model for dense gas dispersion on complex topography. Computer & Geosciences, accepted.

Frondini F., Chiodini G., Caliro S., Cardellini C., Granieri D. and Ventura G. (2004) Diffuse CO_2 degassing at Vesuvio, Italy. Bulletin of Volcanology, 66/7, 642-651, doi:10.1007/s00445-004-0346-x.

Gerlach, T.M, Dokas, M.P., McGee, K.A., 1998. Three-year decline of magmatic CO_2 emissions from soils of a Mammoth Mountain tree kill: Horseshoe Lake, CA, 1995-1997. Geophysical Research Letters, 25 (11), L07615, 1947-1950.

Gianelli G. 1985. On the origin of geothermal CO_2 by metamorphic processes. Bull. Soc. Geol. Italy, 104, 575-584, 1985

Giggenbach, W.F., Sano Y., and Schminckle H.U. 1991. CO_2-rich gases from Lakes Nyos and Monoun, Camerron; Laacher See, Germany; Dieng, Indonesia and Mt. Gambier, Australia – variations on a common theme. J. Volcanol. Geotherm. Res., 45, 311-323.

Giggenbach, W.F., 1990. Water and gas chemistry of Lake Nyos and its bearing on the eruptive process, J. Volcanol. Geotherm. Res., 42, 337-362.

Granieri, D., M. L. Carapezza, G. Chiodini, R. Avino, S. Caliro, M. Ranaldi, T. Ricci, and L. Tarchini (2006) Correlated increase in CO_2 fumarolic content and diffuse emission from La Fossa crater (Vulcano, Italy): Evidence of volcanic unrest or increasing gas release from a stationary deep magma body?. Geophys. Res. Lett., 33, L13316, doi:10.1029/2006GL026460.

Hankin, R.K.S., Britter, R. E., 1999a. TWODEE: the Health and Safety Laboratory's shallow layer

model for heavy gas dispersion. Part 1. Mathematical basis and physical assumptions. J. Hazard. Mater. A66, 211–226.

Hankin, R.K. S., Britter, R E., 1999b. TWODEE: the Health and Safety Laboratory's shallow layer model for heavy gas dispersion. Part 2. Outline and validation of the computational scheme. J. Hazard. Mater. A66, 227–237.

Hankin, R. K. S. , Britter, R. E., 1999c. TWODEE: the Health and Safety Laboratory's shallow layer model for heavy gas dispersion. Part 3. Experimental validation (Thorney island). J. Hazard. Mater. A66, 239–261.

Hankin, R.K. S. 2003a. Heavy gas dispersion: integral models and shallow layer models. Journal of Hazardous Materials, A013, 1-10.

Hankin , R. K. S. 2003b. Shallow layer simulation of heavy gas released on a slope in calm ambient. Part 1: continuous releases. Journal of Hazardous Materials, A103, 205-215.

Hankin , R. K. S. 2003c. Shallow layer simulation of heavy gas released on a slope in calm ambient. Part 2: instantaneous releases. Journal of Hazardous Materials, A103, 217-229.

Hankin 2004a. Major hazard risk assessment over non-flat terrain. Part 1: continuous releases. Atmospheric Environment 38, 695-705.

Hankin 2004b. Major hazard risk assessment over non-flat terrain. Part 2: instantaneous releases. Atmospheric Environment 38, 707-714.

Heinrich, P., Piatanesi, A., Hébert, H., 2001. Numerical modelling of tsunami generation and propagation from submarine slumps: the 1998 Papua New Guinea event. Geophys. J. Int. 145, 97–111.

Jacobson, M., 1999. Fundamentals of atmospheric modelling. 1st edition. Cambridge University Press, New York.

LeGuern, F., Tazieff, H. and Faivre Pierret, R., 1982. An example of health hazard: people killed by gas during a phreatic eruption, Dieng Plateau (Java, Indonesia), February 20th, 1979, Bull.

Volc., 45, 153-156.

Louis, J., 1979. A parametric model of vertical eddy fluxes in the atmosphere. Bounday Layer Meteor. 12, 187-202.

Minissale, A. 2004. Origin, transport and discharge of CO_2 in central Italy. Earth-Science Reviews, 66, 89-141.

National Institute for Occupational Safety and Health (NIOSH), 1997. NIOSH Pocket Guide to Chemical Hazard. DHHS (NIOSH) Publication N. 97-140. Washington, D.C. U.S. Government Printing Office.

National Institute for Occupational Safety and Health (NIOSH), 1981. Occupational Health Guidelines for Chemical Hazards, DHHS (NIOSH) Publication N. 81-123. Washington, D.C. U.S. Government Printing Office.

Oldenburg, C.M. Unger, J.A., 2003. On Leakage and Seepage from Geological Carbon Sequestration Sites: Unsatured Zone Attenuation. Vadose Zone Journal, 2, 287-296.

Oldenburg, C.M. Unger, J.A., 2004. Coupled Vadose Zone and Atmospheric Surface-Layer Transport of Carbon Dioxide from Geologic Carbon Sequestration Sites. Vadose Zone Journal, 3, 848-857.

Rogie, J.D., Kerrick, D.M., Chiodini, G., Frondini, F., 2000. Flux measurements of nonvolcanic CO_2 emission from some vents in central Italy. J. Geophys. Res. 105 (B4), 8435–8445.

Rogie, J.D., Kerrick, D.M., Chiodini, G., Sorry, M.L., Virgili, G., 1998. Continuous monitoring of diffuse CO_2 degassing, Horseshoe Lake, Mammoth Mountain, CA. AGU Fall Mtg., EOS Trans. 79 (45), F941 (suppl.).

Spicer, T., Havens, J., 1989. DEGADIS - DEnse GAs DISpersion Model. Tech. rep., EPA-450/4-89-0019, San Rafael, CA.

Sigurdsson, H., Devine, J.D., Tchoua, F.M., Presser, T.S., Pringle, M.K.W. and Evans, W.C., 1987. Origin of the lethal gas burst from Lake Monoun, Cameroon. J. Volcanol. Geotherm. Res.,

31, 1-16.

Venetsanos, A., Bartzis, J., Wurtz, J., Papailiou, D., 2003. DISPLAY-2: a two-dimensional shallow layer model for dense gas dispersion including complex features. J. Hazard. Mater. A99, 111–144.

Welles, J. M., T. H. Demetriades-Shah, and D. K. McDermitt, Considerations for measuring ground CO_2 effluxes with chambers, Chem. Geol., 177(1– 2), 3 – 13, 2001.

Witlox, H., 1994. The HEGADAS model for ground-level heavy-gas dispersion - i. steady-state model. Atmos. Environ. 28 (18), 2917–2932.

Zalesak, S.T., 1979. Fully multidimensional flux-corrected method transport for fluid. J. Comp. Phys. 31, 335-362.

Acknowledgements. The authors acknowledge the support from funds of the INGV and from the "Dipartimento della Protezione Civile" of Italy in the ambit of INGV-DPC V5 project.

Table 1 - Threshold values for CO_2 concentration in the air

CO_2 thresholds for Human Health	**Principal effect**
5000 ppm (0.5%) TWA (Time Weighted Average - 8 h/day for 5 days per week)[a]	Slight increase in breathing rate
30000 ppm (3%) STEL (Short Term Exposure Limit – 15 min max time exposure four times a day)[a]	Breathing increases to twice normal rate, weak narcotic effect, headache for long time exposure
100000 ppm (10%)[b]	Respiratory distress with loss of consciousness in 10-15 minutes
120000-150000 ppm (12-15%) [b,c]	Lethal concentration, exposure to levels above this is intolerable

[a] National Institute of Occupational Safety and Health (NIOSH), 1997 – Pocket Guide to Chemical Hazard. Publication N. 97-140. Washington, D.C. U.S. Government Printing Office.

[b] Le Guern et al. (1982)

[c] Baxter et al. (1999)

Figure captions:

Fig. 1: Map of Earth degassing in central and southern Italy based on the CO_2 dissolved in the groundwater of regional aquifers (modified after Chiodini et al., 2004). CO_2 fluxes above 0.4 t d^{-1} km^{-2} are related to the presence of deeply derived CO_2 (Collettini et al., 2007). Locations of CO_2 rich gas emissions and main geothermal wells are also reported.

Figure 2: View from above photo of Caldara di Manziana showing the position of the meteorological station (red dot) and the main CO_2 vent . In the top-right corner inset the geographical position of CdM is indicated. In the bottom-right corner inset a zoom of the area around the main CO_2 vent is shown; the CO_2 expulsion from the vent continuously sustains a 0.5 m-high water column.

Fig. 3: Map of CO_2 flux at Caldara on the digital model of the topography as background. The average diffuse degassing flux is about 7.7×10^{-6} kg m^{-2} s^{-1}, whereas the total contribution of the CO_2 vent and the water pool (white dots) is about 0.17 kg s^{-1}.

Fig. 4: Picture of the tower with the stations mounted for meteorological and CO_2 concentration measurements. A cup anemometer was mounted at 3.45 m above the soil; a first temperature sensor was placed at 2.90 m whereas a second sensor was mounted at 0.30 m. The open path infrared CO_2/H_2O analyzer (LI-7500, LI-COR Inc. Lincoln, Nebraska) was mounted at 2.20 m above the ground.

Fig. 5: Comparison between the measured (red dots) and simulated (black lines) CO_2 concentrations averaged every ten minutes. Simulated values are referred to the average concentration over a $25\,\mathrm{m} \times 25\,\mathrm{m}$ square centered at the station.

Fig. 6: Time evolution of concentration at 2.2 m height. Four different time slices are plotted for illustrative purposes. The corresponding meteorological parameters are reported in the top-left corner inset. Effects of both topography and wind are clearly evident in controlling gas accumulation. The complete evolution sequence is shown by the mpeg file “Simulation.mpg”

reported in the electronic appendix.

Fig. 7: Gas concentration maps at the heights of 1.50 m (a) and 0.10 m (b) assuming very low wind stable conditions ($U_a \approx 0.05$ m/s, $z_{ref} / L > 10^3$) for a nighttime duration of ten hours. The total gas flux was assumed to be equal to the measured value (175 td^{-1}). The heights of 0.1 m and 1.5 m were considered as typical levels of inhalation for small-size animals and humans respectively.

Fig. 8: Gas concentration maps at the height of 1.50 m assuming, as in Fig. 7, low wind stable conditions for a nighttime duration of ten hours but considering that the total flux was equal to five times the measured one.

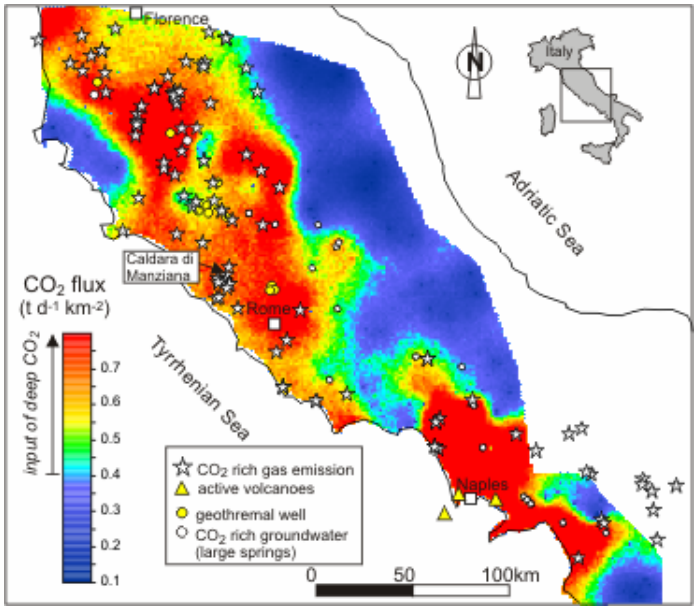

Fig. 1: Map of Earth degassing in central and southern Italy based on the CO_2 dissolved in the groundwater of regional aquifers (modified after Chiodini et al., 2004). CO_2 fluxes above 0.4 t d^{-1} km^{-2} are related to the presence of deeply derived CO_2 (Collettini et al., 2007). Locations of CO_2 rich gas emissions and main geothermal wells are also reported.

Fig. 2: View from above photo of Caldara di Manziana with the position of the meteorological station (red dot) and of the main CO_2 vent in evidence. In the top-right corner inset the geographical position of CdM is shown. In the bottom-right corner inset a zoom of the area around the main CO_2 vent is shown; the CO_2 expulsion from the vent continuously sustains a 0.5-m-high water column.

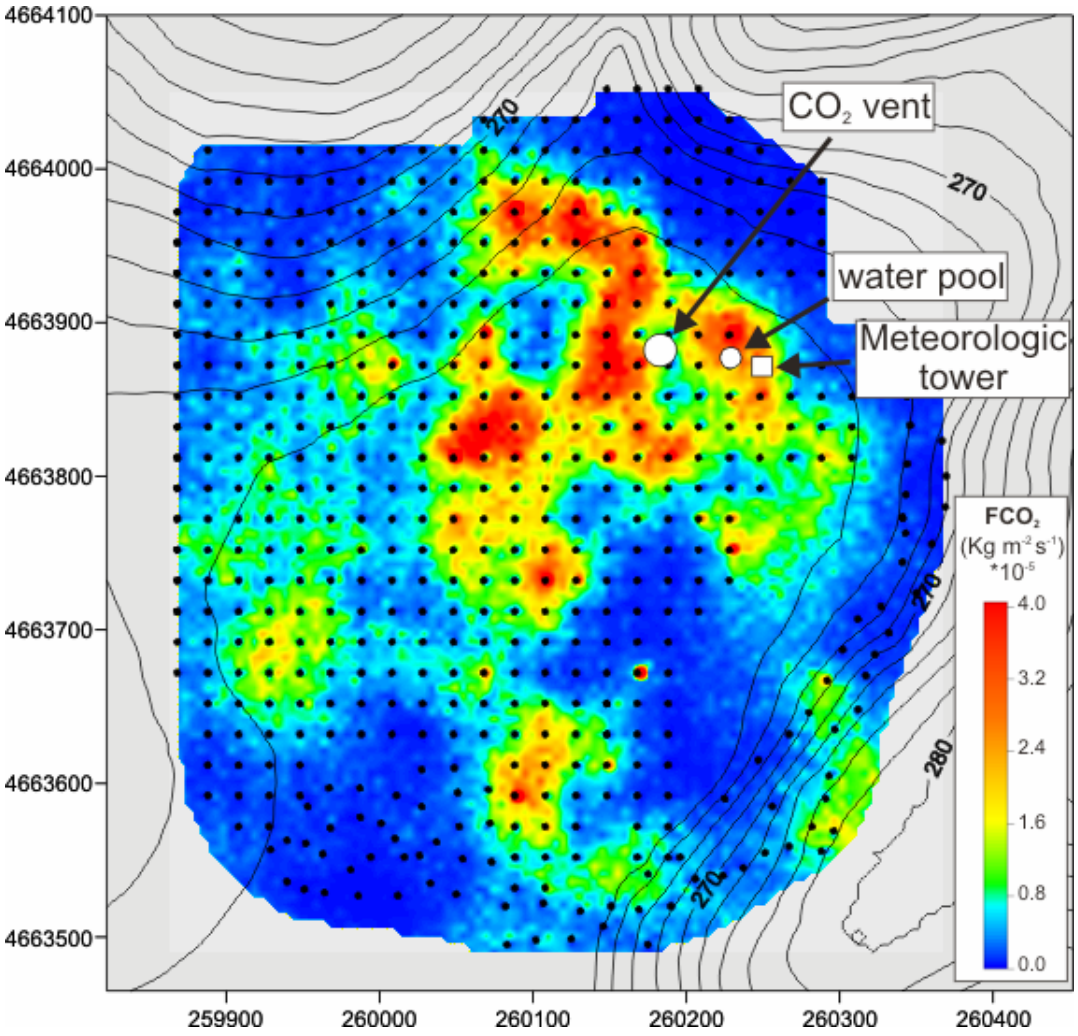

Fig. 3: Map of CO_2 flux at Caldara on the digital model of the topography as background. The average diffuse degassing flux is about 7.7×10^{-6} kg m^{-2} s^{-1}, whereas the total contribution of the CO_2 vent and the water pool (white dots) is about 0.17 kg s^{-1}.

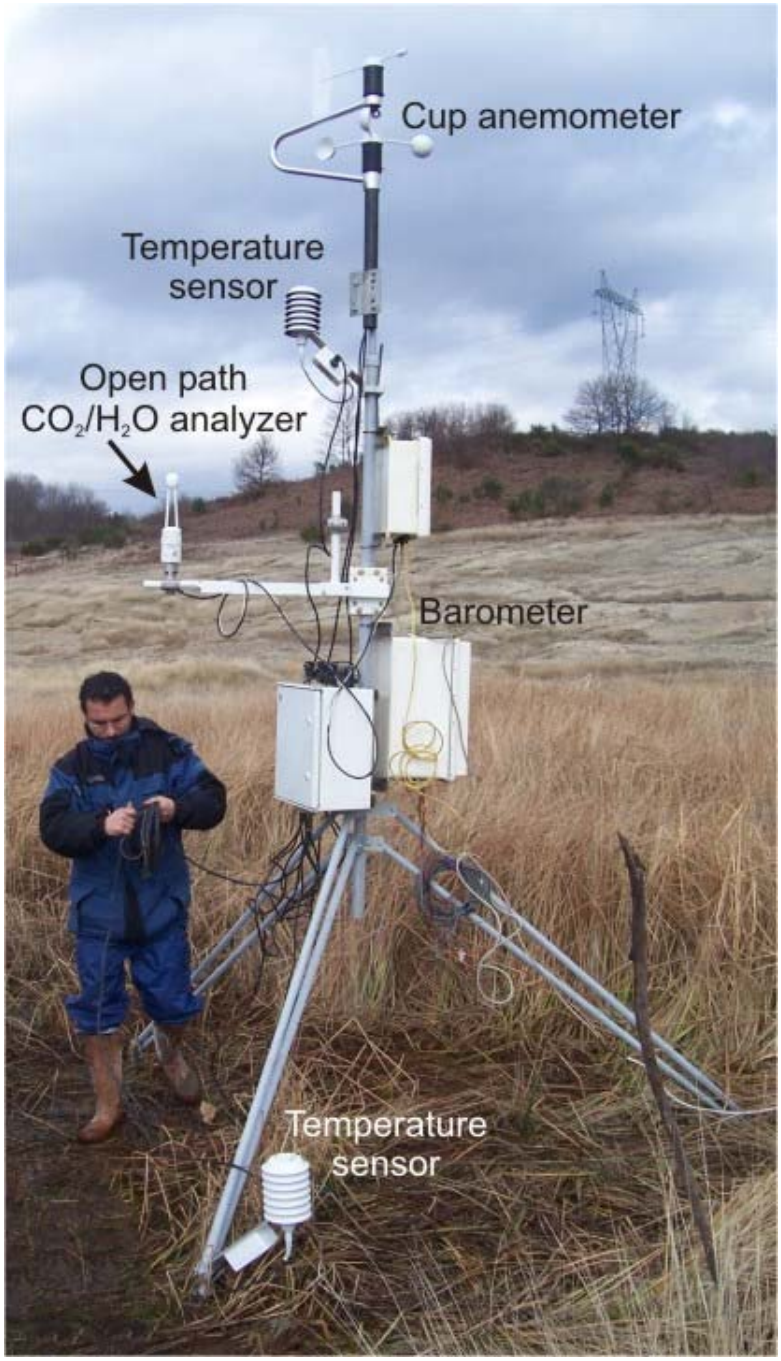

Fig. 4: Picture of the tower with the stations mounted for meteorological and CO_2 concentration measurements. Cup anemometer was mounted at 3.45 m above the soil; a first temperature sensor was placed at 2.90 m whereas a second sensor was mounted at 0.30 m. The open path infrared CO_2/H_2O analyzer (LI-7500, LI-COR Inc. Lincoln, Nebraska) was mounted at 2.20 m above the ground.

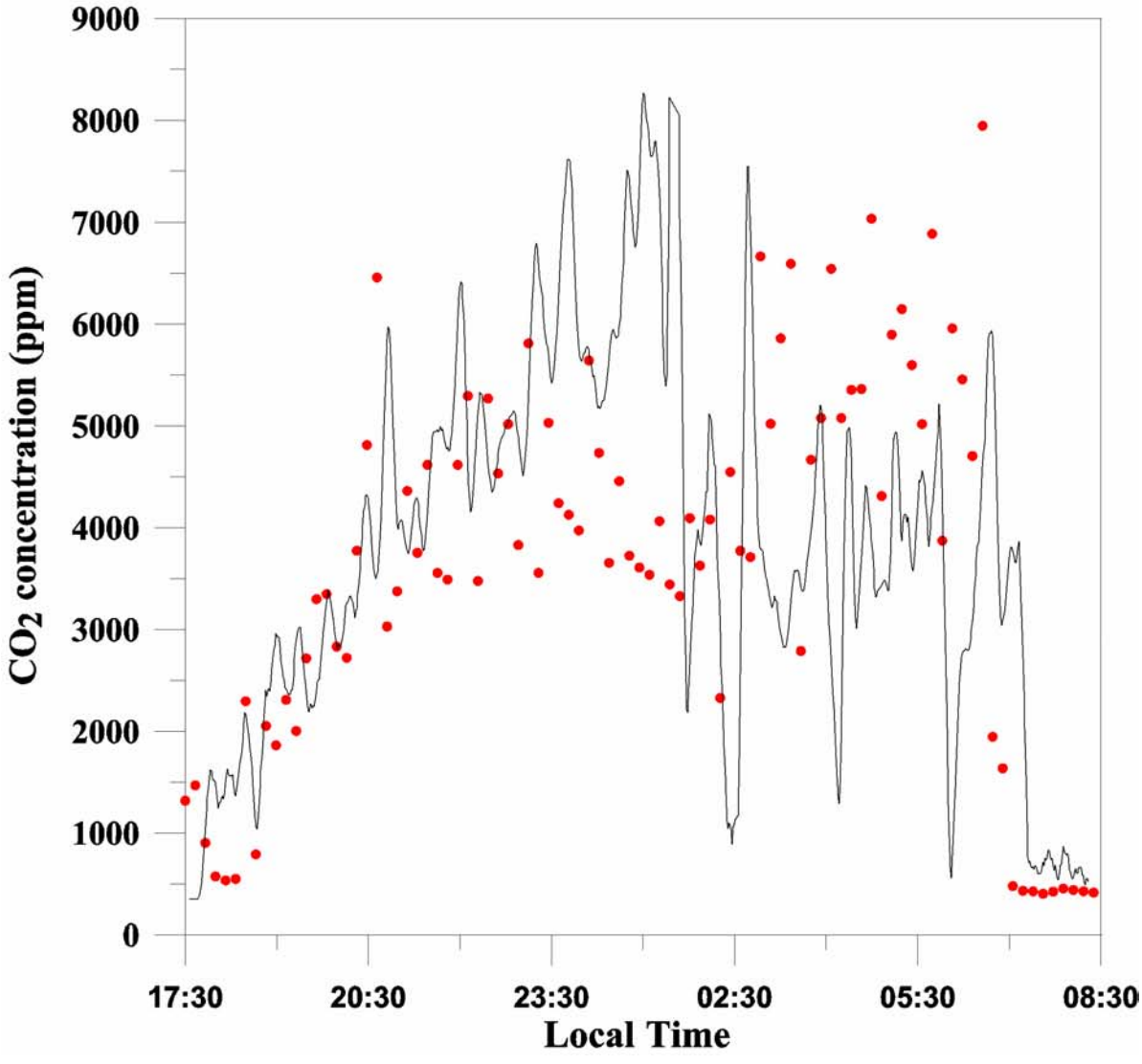
9000
8000
7000
6000
5000
4000
3000
2000
1000
0
CO2 concentration (ppm)
17:30
20:30
23:30
02:30
05:30
08:30
Local Time

Fig. 5: Comparison between the measured (red dots) and simulated (black lines) CO_2 concentrations averaged every ten minutes. Simulated values are referred to the average concentration over a $25\,\mathrm{m} \times 25\,\mathrm{m}$ square centered at the station.

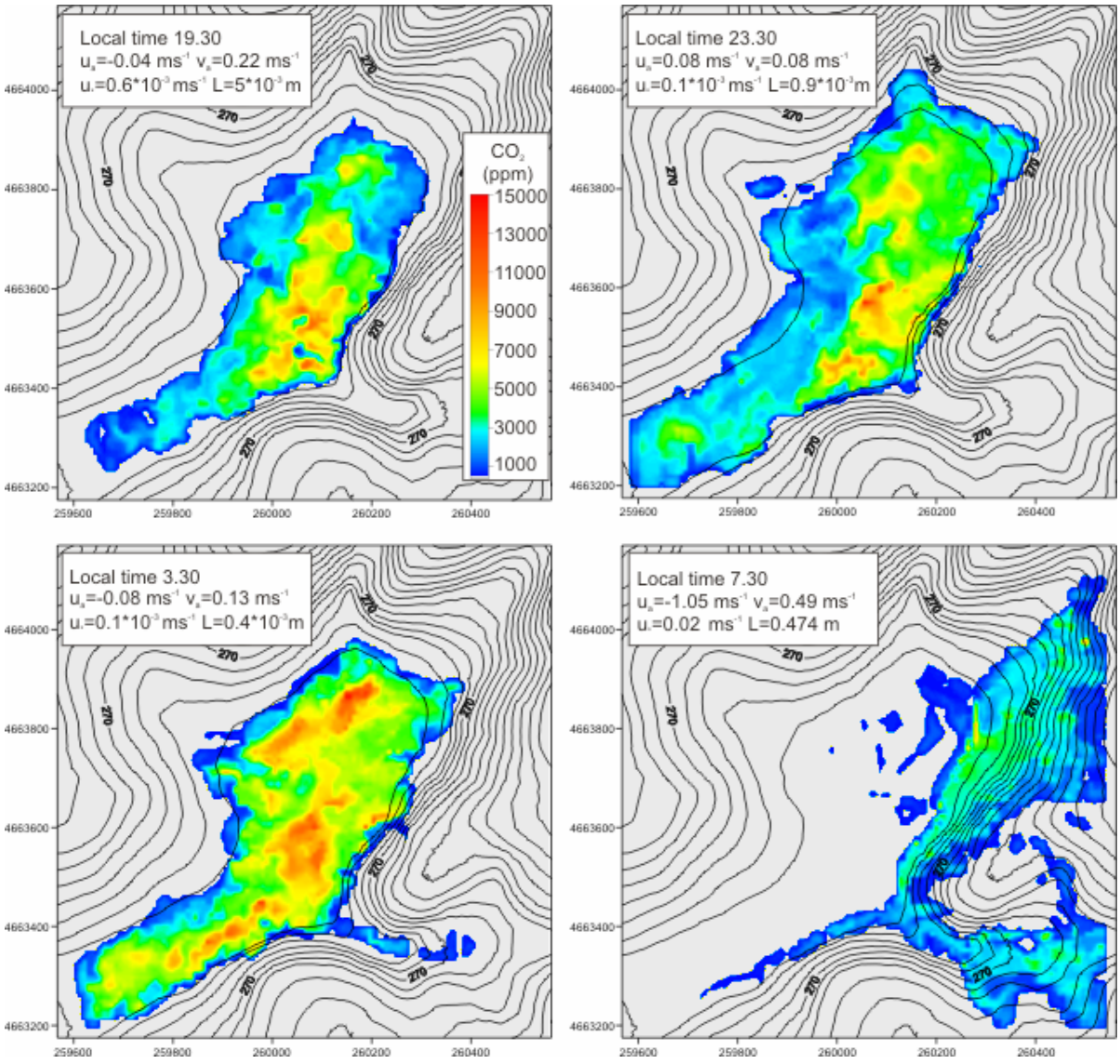

Fig. 6: Time evolution of concentration at 2.2 m. Four different time slices are plotted as examples. Corresponding meteorological parameters are reported in the top-left corner inset. Effects of both topography and wind are clearly evident in controlling gas accumulation. The complete evolution sequence is shown by the mpeg file "Simulation.mpg" reported in the electronic appendix.

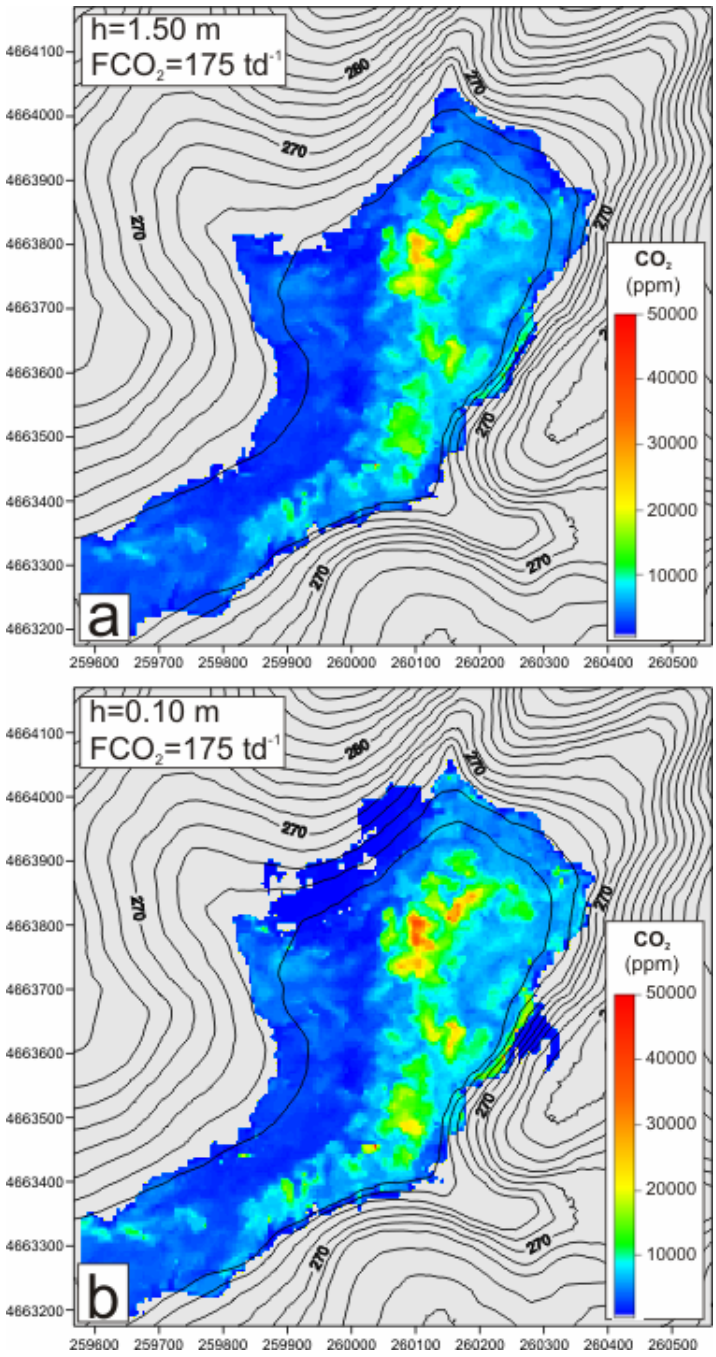

Fig. 7: Gas concentration maps at the heights of 1.50 m (a) and 0.10 m (b) assuming very low wind stable conditions ($U_a \approx 0.05$ m/s, $z_{ref}/L > 10^3$) for a nighttime duration of ten hours. The total gas flux was assumed to be equal to the measured value (175 td^{-1}). The heights of 0.1m and 1.5 m were considered as typical levels of inhalation for small-size animals and humans, respectively.

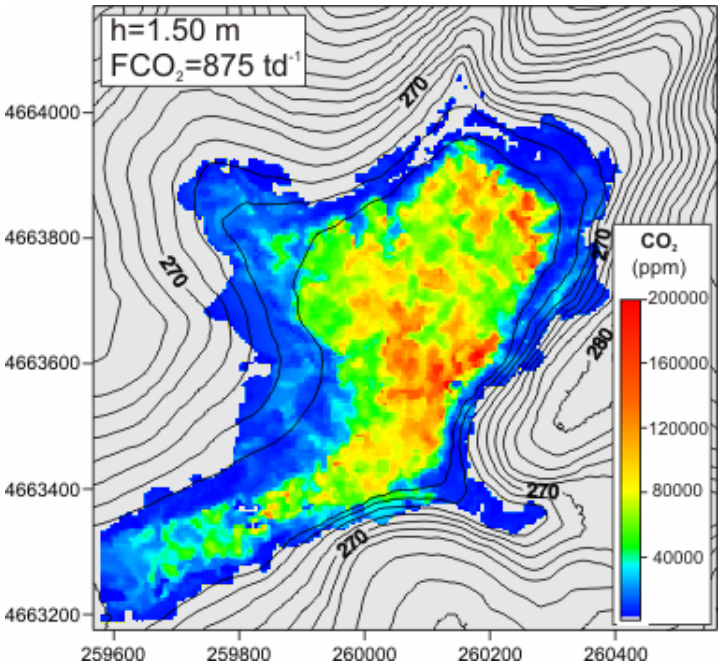

Fig. 8: Gas concentration maps at the height of 1.5 m assuming, as in Fig. 7, low wind stable conditions for a nighttime duration of ten hours but considering that the total flux was equal to five times the measured one.